Chemical Engineering Science 195 (2019) 1–10

Contents lists available at ScienceDirect

Chemical Engineering Science

journal homepage: www.elsevier.com/locate/ces

High-gravity-assisted scalable synthesis of zirconia nanodispersion for light emitting diodes encapsulation with enhanced light extraction efficiency

Xianglei He [a,b], Zhi Wang [a], Yuan Pu [a,b], Dan Wang [a,b,*], Ruijie Tang [a,b], Simin Cui [a,b], Jie-Xin Wang [a,b,*], Jian-Feng Chen [a,b]

[a] State Key Laboratory of Organic Inorganic Composites, Beijing University of Chemical Technology, Beijing 100029, China
[b] Research Center of the Ministry of Education for High Gravity Engineering and Technology, Beijing University of Chemical Technology, Beijing 100029, China

HIGHLIGHTS

- A high-gravity-assisted method for efficient synthesis of zirconia nanoparticles.
- Highly dispersed zirconia nanoparticles in organic solvents and epoxy resin.
- Significant enhanced light extraction efficiency of LEDs by zirconia nanodispersion.

ARTICLE INFO

Article history:
Received 6 October 2018
Received in revised form 12 November 2018
Accepted 15 November 2018
Available online 16 November 2018

Keywords:
Zirconia nanoparticles
Rotating packed bed
Hybrid nanocomposite
LED encapsulation

ABSTRACT

Zirconia-based hybrid polymers has become one of the ideal encapsulation material for light emitting diodes (LEDs) with high extraction efficiency due to their proper refractive index to those of semiconductor chips. However, the controlling of the dispersion for zirconia nanoparticles in polymeric hosts to obtain optically transparent hybrid nanocomposites has been one of the major challenges. Herein, we reported the synthesis of zirconia nanodispersion *via* high-gravity-assisted homogeneous precipitation in an internal circulation rotating packed bed (RPB) reactor followed by two-step modification. An alternative to conventional precipitation in batch stirred tank reactors (STR), the process intensification by high-gravity RPB results in homogeneous micromixing during the nucleation and growth of zirconia particles, which are benefit for continuous and reproducible production of ultrasmall zirconia nanoparticles. The obtained zirconia nanoparticles are purely cubic phase with narrow size-distribution in the range of 3–5 nm according to the X-ray diffraction and transmission electron microscopy characterization, which were similarity to that by the conventional methods. Nevertheless, the average hydrodynamic diameters of zirconia nanoparticles in aqueous solutions obtained by RPB methods were much smaller than those prepared in conventional STR, which enabled easy control and surface modification for highly dispersed nanodispersion in organic solvents and/or polymeric hosts. After two-step surface modification, zirconia nanoparticles with goal-directed structures were obtained, with highly dispersity in various organic solvents (e.g. toluene, trichloromethane, tetrahydrofuran, etc.) and aliphatic epoxy resin, forming transparent hybrid films with tunable refractive indexes. The preliminary applications of these zirconia nanodispersions for LEDs encapsulation were demonstrated. The light extraction efficiency of the LEDs devices packaged with zirconia/epoxy hybrid material increased by 10 percent when the doping content of zirconia nanoparticles was 0.2, compared to the devices encapsulated by original epoxy.

© 2018 Elsevier Ltd. All rights reserved.

1. Introduction

Zirconia is an excellent refractory and ceramic material with high mechanical strength, fracture toughness, heat tolerance, high melting point, resistance to abrasion and thermal-shock (Chiang, 2015; Enomoto et al., 2018), which has found widely applications such as automobile engine parts, gas turbine parts, high tempera-

* Corresponding authors at: State Key Laboratory of Organic Inorganic Composites, Beijing University of Chemical Technology, Beijing 100029, China.
E-mail addresses: wangdan@mail.buct.edu.cn (D. Wang), wangjx@mail.buct.edu.cn (J.-X. Wang).

https://doi.org/10.1016/j.ces.2018.11.036
0009-2509/© 2018 Elsevier Ltd. All rights reserved.

ture pigments, cutlery and refractory crucible. In particular, cubic zirconia nanocrystals are very promising as fillers of flexible polymers based transparent nanocomposites with tunable refractive index for encapsulation of optical devices to enhance the light extraction efficiency and save energy (Chung et al., 2016; Enomoto et al., 2017; Lee et al., 2008; Lei et al., 2014; Lin et al., 2018). However, the controlling of the dispersion for nanoparticles in polymeric hosts to avoid the scattering of large aggregated particles and obtain optically transparent hybrid nanocomposites are challenging (Chiang, 2015). Therefore, the development of scalable methods for the synthesis highly dispersed sub-10 nm zirconia nanoparticles in various solvents and/or polymer hosts has been one of key materials challenge in moving toward their commercialization and advanced applications (Huang et al., 2017).

One common synthetic method for the synthesis of highly dispersed ultrasmall zirconia nanoparticles is based on the thermal decomposition of organic zirconium precursors in organic solvents (Garnweitner et al., 2007; Tao et al., 2013). However, the organic zirconium precursors are usually expensive and the use of organic solvents results in a large amount of organic liquid wastes, which limit the scale-up production of zirconia nanoparticles. Another approach for preparation of zirconia nanoparticles is based on the liquid precipitation between soluble inorganic zirconium salts and alkali followed by hydrothermal crystallization and surface modification (Chang et al., 2012; Huang et al., 2011; Li et al., 2008; Xia et al., 2018). The aqueous synthesis of zirconia nanoparticles in water offers the following advantages: (1) it uses relatively inexpensive zirconium precursors and less toxic organic reagents that are beneficial for commercial production; (2) covalent binding of zirconia nanoparticles with various organic groups are function-oriented to improve the compatibility between the nanoparticle and surrounding matrix for optimum properties. Nevertheless, the conventional precipitation process of zirconia precursors is usually performed in batch-type stirred tank reactors (STR) with low efficiency of fluid mixing and mass transfer, in which the nucleation of nanoparticles are hard to occur uniformly, especially when large volumes of solution are involved (Pu et al., 2018a). Therefore, a major challenge for scalable production of highly dispersed zirconia nanodispersion is the realization of homogenous synthesis conditions in the reactors for precipitation and crystallization, which is indispensable to achieve high quality zirconia nanoparticles with less aggregates, namely small hydrodynamic diameters in aqueous solutions, for subsequent surface modification.

Along with the development of green chemical engineering focusing on the design of chemical reaction processes for green product and green process, a variety of methods for continuous and reproducible production of nanoparticles by process intensification have emerged (Chen, 2017; Wang et al., 2017). As one of the cutting-edge process intensification technologies, the high-gravity technology facilitates the fulfillment of these demands as the use of rotating packed bed (RPB) reactors allow fast mass transfer and molecular mixing (Wenzel and Gorak, 2018), resulting in good controllability of the synthesis parameters. In addition, the RPB system can be operated continuously and are ease to yield larger mass-fluxes for scale-up (Huang et al., 2018; Kuang et al., 2015; Zhao et al., 2010). Along with others, we have demonstrated that the high-gravity technology is highly promising platform for the production of various types of micro- and nanopowders of metal oxides (Jiao et al., 2017; Leng et al., 2017; Yang et al., 2017; Zhao et al., 2018). Meanwhile, a few works have investigated the synthesis of nanodispersion of insoluble inorganic metal compounds in organic media (Kang et al., 2018; Pu et al., 2018b). The high-gravity-assisted synthesis of zirconia nanodispersion aiming for hybrid encapsulation of light emitting diodes (LEDs) to the best of our knowledge has rarely been reported.

In this study, we establish the synthesis of zirconia nanoparticles in a high-gravity internal circulation RPB reactor with a view to the process intensification for scalable ability of large production. Therefore, the detailed studies on the effects of high-gravity levels and reaction time were investigated to confirm the optimal conditions. A two-step surface modification approach were developed for tailoring of the zirconia nanoparticles to improve the compatibility between the zirconia nanoparticle and surrounding aliphatic epoxy resin for transparent hybrid encapsulation of LEDs devices. Characterization of the zirconia nanoparticles showed much smaller hydrodynamic diameters in aqueous solutions than those obtained by a conventional STR route, resulting in higher dispersed zirconia nanodispersion in organic solvents and polymeric hosts. Compared to the devices encapsulated by commercial epoxy, the use zirconia nanodispersions for zirconia/epoxy hybrid encapsulation benefited the light extraction efficiency of LEDs, increasing up to 10 percent. This study demonstrated that the newly developed high-gravity-assisted scalable synthesis approach stands for an effective method for highly dispersed sub-10 nm zirconia nanoparticles in moving toward their commercialization and advanced applications in optical devices for saving energy.

2. Materials and methods

2.1. Materials

Zirconium carbonate basic (ZCB), 3-(Trimethoxysilyl)propyl methacrylate (KH570), methylhexahydrophthalic anhydride (MHHPA) and 3,4-epoxycyclohexylmethyl 3,4-epoxycyclohexane carboxylate (epoxy) were purchased from Sigma-Aldrich. Other chemicals including ammonium bicarbonate, sodium hydroxide, butyric acid (BA), trichloromethane (TCM), dichloromethane (DCM), tetrahydrofuran (THF), methyl isobutyl ketone (MIBK), acetyl acetone (Hacac) and toluene were obtained from Shanghai Macklin Biochemical Co., Ltd. All the chemicals were used without any additional purification and deionized water was used for all experiments.

2.2. Synthesis of ZrO_2 nanoparticles

For the synthesis of ZrO_2 nanoparticles, an internal circulation RPB reactor (Fig. 1) was used for the precipitation and crystalliza-

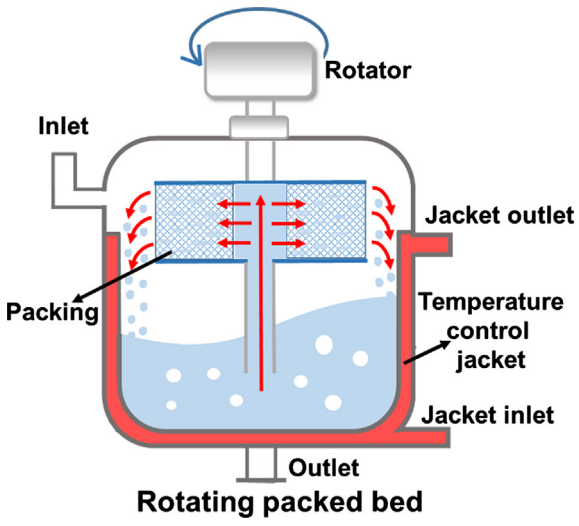

Fig. 1. Schematic diagram of the internal circulation RPB reactor. Red lines and arrows indicate the flow of reactants. (For interpretation of the references to color in this figure legend, the reader is referred to the web version of this article.)

tion process. The RPB reactor consists of a packed rotator, a motor, a temperature-control jacket, a seal ring, a lifter, an inlet and an outlet. In a typical experiment, 40 g NaOH were dissolved in 200 mL water and maintained at 80 °C to form solution A. Meanwhile, 40 g ZCB were added into 200 mL water, stirring at 80 °C for 10 min to obtain suspension B. The two solutions were simultaneously added into inlet of the RPB reactor for mixing and precipitation. After the feeding of solution A and suspension B, the mixture was then allowed for crystallization inside the internal circulation RPB reactor for certain time. In our experiments, we investigated the effects of high gravity levels and the cycle time on the particle sizes of ZrO_2 nanoparticles. The high gravity levels were controlled by adjusting the rotation speeds of the RPB in the range of 500–1500 rpm (revolutions per minute). For the internal circulation RPB reactor used in our experiments, the inner radius of the packing is 0.034 m and the outer radius of packing is 0.1 m. The corresponding mean high-gravity levels (β) were 20, 81 and 182 at various rotation speeds of 500, 1000 and 1500 rpm, respectively, as calculated by equation (Wu et al., 2018; Wu et al., 2016):

$$\beta = \frac{\int_{r_1}^{r_2} 2\pi r\beta dr}{\int_{r_1}^{r_2} 2\pi r dr} = \frac{2\omega^2(r_1{}^2 + r_1 r_2 + r_2{}^2)}{3(r_1 + r_2)g}$$

where r_1,r_2, and ω are inner radius of packing (m), outer radius of packing (m) and rotor speed (rad/s), respectively. The g is the gravity acceleration and the value of this number is 9.8 m/s^2.

The effects of the cycle time on the particles crystallization and growth were investigated at time points of 1–6 h at one hour intervals. The as-prepared ZrO_2 nanoparticles were then washed twice with water and 1 mol/L ammonium bicarbonate solution. The suspension liquid was separated by centrifugation (5000 rpm for 5 min) and the slurry of ZrO_2 nanoparticles was obtained. In one experiment, 25 g of slurry was obtained, and the slurry contained some free water, bound water, and carbonic acid groups, wherein the weight of the dry zirconia was 15 g. The ZCB used in the raw material has a zirconia content of 40% or more, and theoretically, the weight of zirconia is 16 g or more. The theoretical zirconium atom conversion of this reaction is 100%, and the difference between the actual value and the theoretical value is mainly due to the fact that a plurality of centrifugal washing processes carry away a part of the zirconia product. As the control experiment, the ZrO_2 nanoparticles were obtained by mixing of solution A and suspension B in a conversional stirred tank reactor (STR) composed of a beaker and a stirrer working at 500 rpm. The ZrO_2 nanoparticles were prepared after reacting for 5 h in STR followed by same washing process as the RPB experiment.

2.3. Two-step surface modification of ZrO_2 nanoparticles.

The slurry of ZrO_2 nanoparticles (25 g) were re-dispersed in 25 mL of water and then added into 100 mL of BA. The mixture was maintained at 70 °C for 10 h and was then centrifuged and washed twice with water. The white powder of BA-capped ZrO_2 nanoparticles (18 g) were obtained by vacuum-drying the precipitate at 110 °C for 6 h. The particles could be easily dispersed in toluene and form transparent dispersion even at solid content of 70 wt%. The BA-capped ZrO_2 nanoparticles were then modified by maintaining the particles with excess KH570 in toluene at 60 °C for 2 h. After the replacement of BA by KH570, an equal amount of water was used to extract the BA released from the surface and possibly some residual salts by centrifugation (5000 rpm for 5 min). After vacuum drying at 80 °C for 4 h, the white powder of KH570 modified ZrO_2 nanoparticles (19 g) were obtained, which can be easily re-dispersed in various organic solvents including toluene, THF, MIBK, TCM, DCM and Hacac.

2.4. Preparation of ZrO_2/epoxy hybrid nanocomposites

The ZrO_2/epoxy hybrid nanocomposites were then prepared *via* co-solvents methods. Briefly, a certain amount of KH570 modified ZrO_2 nanopowder was dispersed in 2 mL of toluene to form transparent ZrO_2 nanodispersion with different solid contents. 1 g of epoxy as dissolved in 2 mL of toluene to form transparent solution. The two solutions were then mixed under magnetic stirring for 5 h. The color of the mixture was white initially, but after sufficient stir it gradually became transparent solution. After that, the toluene was removed by vacuum drying at 65 °C. Then add 1 g MHHPA as a hardener to the composite epoxy resin. The hybrid epoxy-based resins were cured at 75 °C for 0.5 h and then 120 °C for 1.5 h in PTFE molds. The amounts of KH570 modified ZrO_2 nanoparticles were set as 0 g, 0.11 g, 0.22 g, 0.50 g, 0.86 g, and 2 g to prepare hybrid films with ZrO_2 contents of 0, 5, 10, 20, 30, and 50 wt%, respectively.

2.5. Characterization

The transmission electron microscope (TEM) images were taken by a Hitachi HT-7700 TEM operating at bright field mode with an accelerating voltage of 120 kV. Histograms of the particle size distributions were obtained by a software which called Nano Measurer. The high-resolution TEM images were recorded in a Hitachi H-9500 TEM operating at 300 kV in bright-field mode. The hydrodynamic diameters of the particles were determined by dynamic light scattering (DLS) measurements using a Malvern Zetasizer Nano ZS90 instrument. The study of chemical structure of the modifiers on ZrO_2 was employed by ^{1}H nuclear magnetic resonance (NMR) spectroscopy (AvanceII 300, Bruker). The X-ray diffraction (XRD) patterns of the samples were measured by a Shimadzu XRD-6000 diffractometer. The Raman spectra were measured by a Renishaw inVia micro-Raman spectroscopy system excited by a 514 nm laser. A PerkinElmer spectrum GX FTIR spectroscopy system was used to record the FITR spectra of solid samples. Thermogravimetric analysis (TGA) was performed by using a Q50 TGA from TA Instruments. A Shimadzu UV-2600 UV–Vis spectrometry was used to measure the UV–Vis transmittance spectra. The refractive indexes were measured with an Abbemat 300 Abbe refractometer. The light extraction efficiency of LEDs devices were measured by the Everfine LEDspec system.

3. Results and discussion

The formation process of ZrO_2 nanoparticles was shown schematically in Fig. 2. Firstly, the growth of -Zr-O-Zr- networks occurred *via* the hydrolysis and condensation reaction of ZCB in the strong alkaline environment of pH = 13 (Singhal et al., 1996). The nanosized ZrO_2 particles were then prepared by further crystallization and dehydration under thermal treatment (Chung et al., 2016). Due to the presence of carbonate groups on the surface, the growth of ZrO_2 particles was limited, forming ultrasmall particles with abundant surface groups (Chiang et al., 2016). The effects of reaction time on the crystallization and dehydration process of ZrO_2 particles in RPB were investigated. The results of XRD shown in Fig. 2b demonstrate that diffraction intensity increased with the reaction time while the crystallization quality of ZrO_2 will be also improved. The diffraction peaks of at 30.1°, 35.0°, 50.2°, and 59.7° corresponding to the ZrO_2 crystal planes of (1 1 1), (2 0 0), (2 2 0), and (3 1 1) respectively, were observed from the XRD patterns. When the reaction time reaches 5 h, no significant change in XRD patterns were observed. Therefore, the optimized reaction time for RPB route was 5 h in our experiments. The Raman scattering spectrum reveals the characteristic peak of cubic ZrO_2 at 500–

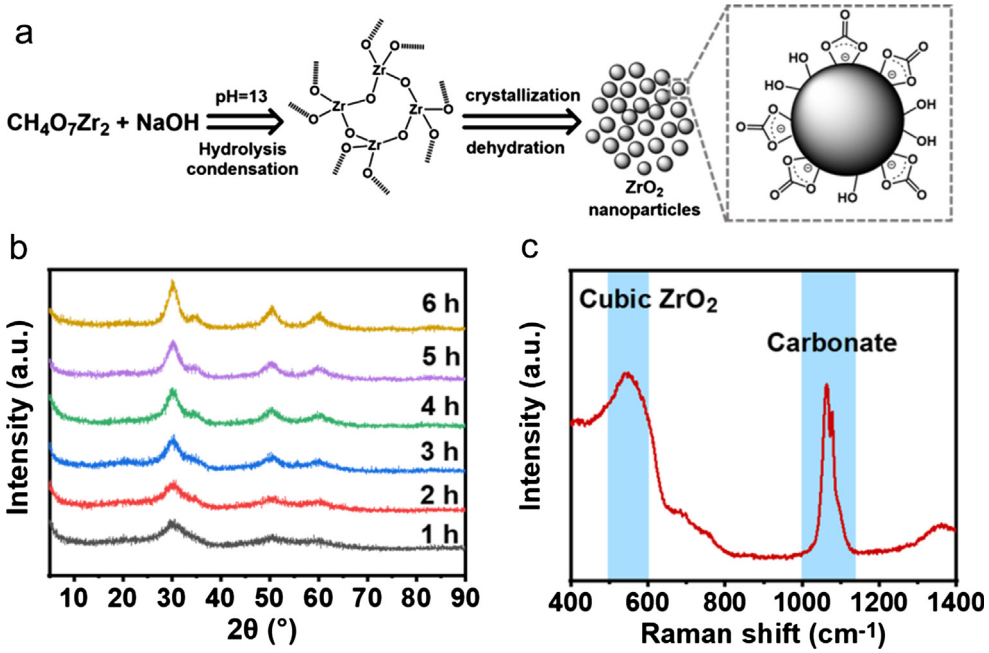

Fig. 2. (a) Schematic diagram for the formation process of ZrO_2 nanoparticles. (b) XRD patterns of the samples obtained from RPB with reaction time of 1, 2, 3, 4, 5 and 6 h, respectively. (c) Raman spectrum of the sample prepared from RPB with reaction time of 5 h.

600 cm^{-1} and the carbonate at 1000–1100 cm^{-1}, proving another evidence for the formation of cubic ZrO_2 (Fig. 2c).

Preliminary comparison on the morphology and dispersion behavior of synthetic ZrO_2 obtained by RPB and STR (reaction time = 5 h) were shown in Fig. 3. All the samples were prepared by dipping copper grids in respective aqueous dispersions with solid content of 0.002 wt% and were observed at different levels of magnification. TEM images indicate that the existence of a large amount of agglomerations for the ZrO_2 powder obtained by conversion STR with irregular shape in the size range of 1–5 μm (Fig. 3a–c). It was obvious that the use of RPB had a great effect on disagglomeration of ZrO_2 nanopowders (Fig. 3d–f). Although a few agglomerations in the range of several hundreds of nanometers were observed, most of the ZrO_2 nanoparticles obtained by RPB route were monodisperse (Fig. 3f). The hydrodynamic diameters of ZrO_2 nanoparticles obtained by STR (stirring rate = 500 rpm) and RPB routes (high gravity level β = 20, 81, 182) were investigated by DLS measurements. These results shown in Fig. 3i demonstrates that the relationship hydrodynamic dispensability of ZrO_2 nanoparticles in aqueous solution had positive relation with the high gravity levels of the preparation conditions. The particles obtained by mixing in the STR showed an average hydrodynamic diameter of 1000 nm. However, the particles obtained by mixing in RPB reactors exhibited much smaller hydrodynamic diameters than those obtained in the STR. The hydrodynamic diameters were 306, 253 and 124 nm for the high gravity level of 20, 81 and 182, respectively. The XRD patterns of samples obtained at various high gravity levels exhibited similar shape and intensity (Fig. S1). These results indicated that the high gravity level of the RPB has influenced the hydrodynamic sizes of the re-dispersed ZrO_2 nanoparticles in aqueous solutions but had no effect on the crystallization of the particles. As the high gravity levels increasing, the micromixing and mass transfer of the reactants become more homogeneous, resulting in ZrO_2 nanoparticles with more uniform bidentate carbonate groups on the surface, which is the key factor affecting the agglomeration of ZrO_2 nanoparticles. More hydrophilic groups on the nanoparticles result in lower surface energy, higher dispersibility and weaker trends for aggregation in aqueous solutions. Therefore, the hydrodynamic diameters of the re-dispersed ZrO_2 nanoparticles in aqueous solutions decreased as the increase of high gravity levels for the preparation process in RPB reactors. However, the crystallization of ZrO_2 nanoparticles were relatively slow reactions, which was no obvious affected by the micromixing and mass transfer efficiency. Since high dispersibility of nanoparticles is beneficial for the surface modification, the optimized high gravity level for RPB route in our experiments was 182. More related works, including the designing of reactors with higher gravity levels and processing capacities, analytical and feedback mechanisms for real-time tuning and optimization of products, are helpful to achieve high-quality ZrO_2 nanoparticles and for scale-up, which should be good topics for future studies.

Epoxy resin has been among the most widely used LEDs encapsulation material (Chen et al., 2015; Chung et al., 2012; Tao et al., 2013). In this work, two-step surface modification was introduced to transfer the aqueous dispersible ZrO_2 nanoparticles into organic solvents and water insoluble epoxy matrix, by grafting the ZrO_2 nanoparticles with BA and KH570 molecules. During the first step reaction, the BA molecules were covalently attached to the ZrO_2 nanoparticles *via* the reaction between hydroxyl and carboxyl groups (Chiang et al., 2016), forming BA capped ZrO_2 (ZrO_2@BA) nanoparticles (Fig. 4a). After surface modification with BA, the ZrO_2 nanoparticles obtained from conversional STR route (STR-ZrO_2@BA) exhibited high dispersibility than the original particles. The DLS measurements of STR-ZrO_2@BA demonstrate an average hydrodynamic diameter of 20 nm for the particles in toluene (Fig. 4b). In stark contrast, the BA capped ZrO_2 nanoparticles obtained from optimized RPB route (RPB-ZrO_2@BA) were with an average of hydrodynamic diameter of 10 nm in toluene (Fig. 4b). The TEM image of RPB-ZrO_2@BA demonstrated that the particles were monodisperse (Fig. 4c). The ^{1}H NMR spectrum of ZrO_2@BA nanoparticles indicate the BA molecules are grafted onto the surface of zirconia because hydrogen atoms in three different chemical environments are detected to be consistent with BA molecules (Fig. S2). Due to the BA binding on the surface, the ZrO_2@BA nanoparticles could be dispersed in organic solvent such as toluene (Fig. S3).

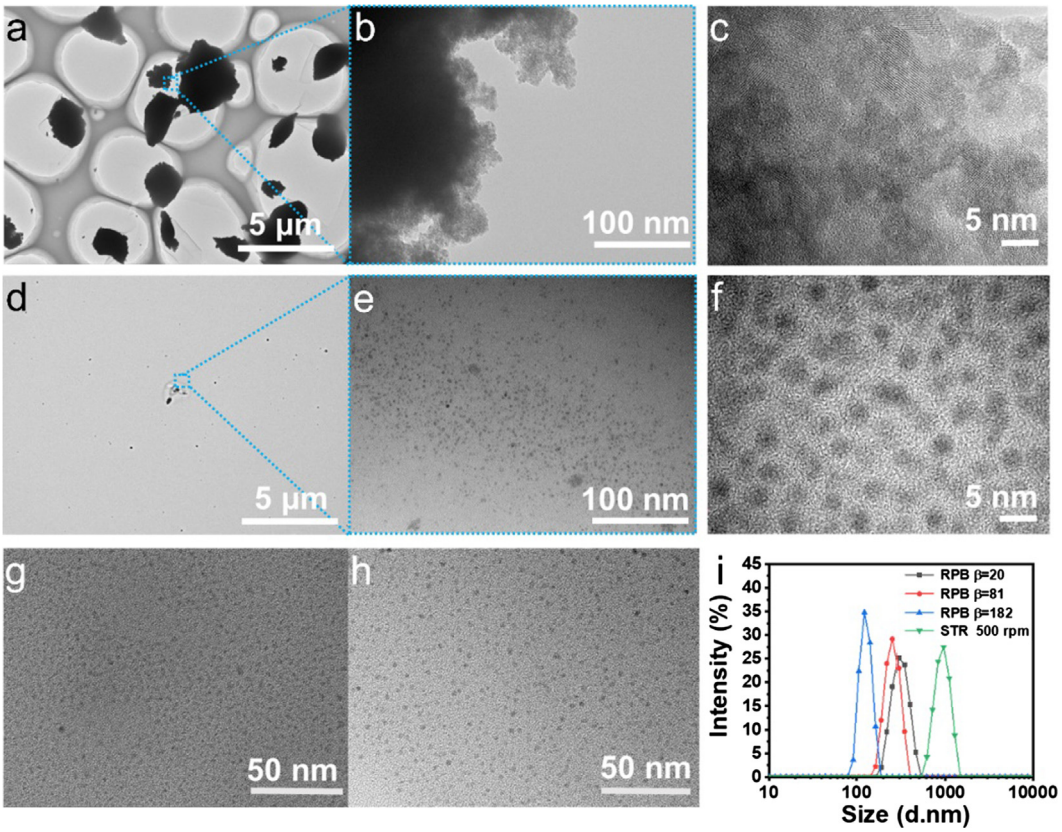

Fig. 3. TEM images at different levels of magnification for ZrO_2 nanoparticles obtained by (a–c) STR route and (d–f) RPB route (β = 20). TEM images of ZrO_2 nanoparticles obtained by RPB route with high gravity level of (g) β = 81 and (h) β = 182. (i) DLS results of the samples in (a, d, g, h).

However, they were hardly dispersed in epoxy resin for hybrid encapsulation materials of LEDs devices.

To further improve the compatibility between the ZrO_2@BA nanoparticle and surrounding aliphatic epoxy resin, the KH570 molecules were then introduced to the surface of ZrO_2@BA as the second step modification based on the reaction between hydroxyl and silicon methoxy (Fig. 5a) (Chung et al., 2016). The XRD patterns of the ZrO_2 nanoparticles, ZrO_2@BA nanoparticles and ZrO_2@BA-KH570 nanoparticles shown in Fig. 5b indicate similar crystal structure of cubic ZrO_2, demonstrating the crystal structure of the ZrO_2 nanoparticles was stable during the two-step modification process. The ^{1}H NMR spectrum of ZrO_2@BA-KH570 nanoparticles demonstrated the presence of both BA and KH570 structures (Fig. S4). The FTIR spectra of these samples are given in Fig. 5c. The peaks at 1575 cm^{-1} and 1350 cm^{-1} observed from the FTIR spectrum of ZrO_2 nanoparticles were attributed to the carbonate groups on the surface. After modification with BA, new bands appeared at 1700 cm^{-1}, 1366 cm^{-1} and 1240 cm^{-1} for the stretching of C═O, CH_3 and C—O groups of BA, respectively. For the sample of ZrO_2@BA-KH570, the stretching of Si—O—Zr band form 800–1000 cm^{-1}, indicated the bonding of the KH570 on the ZrO_2 surface (Su and Chen, 2008). According to the TGA results shown in Fig. 5d, the residue ZrO_2 was 85.6 wt% after heating to 800 °C of the unmodified ZrO_2 nanoparticles and the weight loss was mainly attributed to the carbonate groups on the surface of ZrO_2 NPs. The residue ZrO_2 was 78.9 wt% and 82.1 wt% after heating to 800 °C from the ZrO_2@BA-KH570 nanoparticles and ZrO_2@BA nanoparticles, respectively. Combined with the analysis of ^{1}H NMR spectrum (Fig. S4), the KH570/BA ratio in the ZrO_2@BA-KH570 was calculated to be 2.64.

Due to the compatibility of KH570 molecule structure with organic solvents, the ZrO_2@BA-KH570 nanoparticles could be dispersed well in toluene, forming transparent nanodispersion with solid contents of up to 50 wt% (Fig. 6a), giving a clear view of the patterns behind the bottles. They can also be dispersed well in a variety of organic solvents such as THF, TCM, DCM, MIBK and Hacac (Fig. 6b). The DLS results show that the average hydrodynamic particle sizes in different organic solvents were similar around 10 nm (Fig. 6c). The typical UV–vis absorbance spectrum of ZrO_2@BA-KH570 nanodispersion (1 wt% in toluene) is shown in Fig. S5, in which no significant absorbance and/or scattering were observed in the range of visible light. These results indicated the low degree of association between ZrO_2@BA-KH570 particles.

Fig. 7a presents the digital photos of ZrO_2/epoxy hybrid nanocomposites prepared *via* co-solvents methods. The thickness of all the films were the same as 0.25 mm and the weight ratios of ZrO_2@BA-KH570 nanoparticles doped in the hybrid films were 0, 5, 10, 20, 30, 50 wt%, respectively. It can be seen that all the hybrid films were optical transparent in the range of visible light without significant absorption and scattering. The transmittance spectra of the films demonstrate that the transmittance of light at wavelength of 500 nm for the films with ZrO_2@BA-KH570 nanoparticles doping ratio of less than 30 wt% are higher than 97%. Compared with pure epoxy resin, the addition of ZrO_2 causes an absorption in the wavelength range from 250 nm to 300 nm (Fig. S5), and the absorption becomes more significant with an increase in the ZrO_2 content (Yamada et al., 2000). Moreover, a plunge in the wavelength range form 300 to 400 nm was demonstrated in the spectra of epoxy/ZrO_2 nanocomposite. This is due to the coordination of the butyric acid, KH570, and epoxy itself (Chung et al., 2016; Chung et al., 2012; Enomoto et al., 2015). The transmittance of hybrid films with ZrO_2@BA-KH570 doping ratio of 50 wt% exhibited significant decreased values (~80% at wavelength of 500 nm), which was attributed to the scattering of

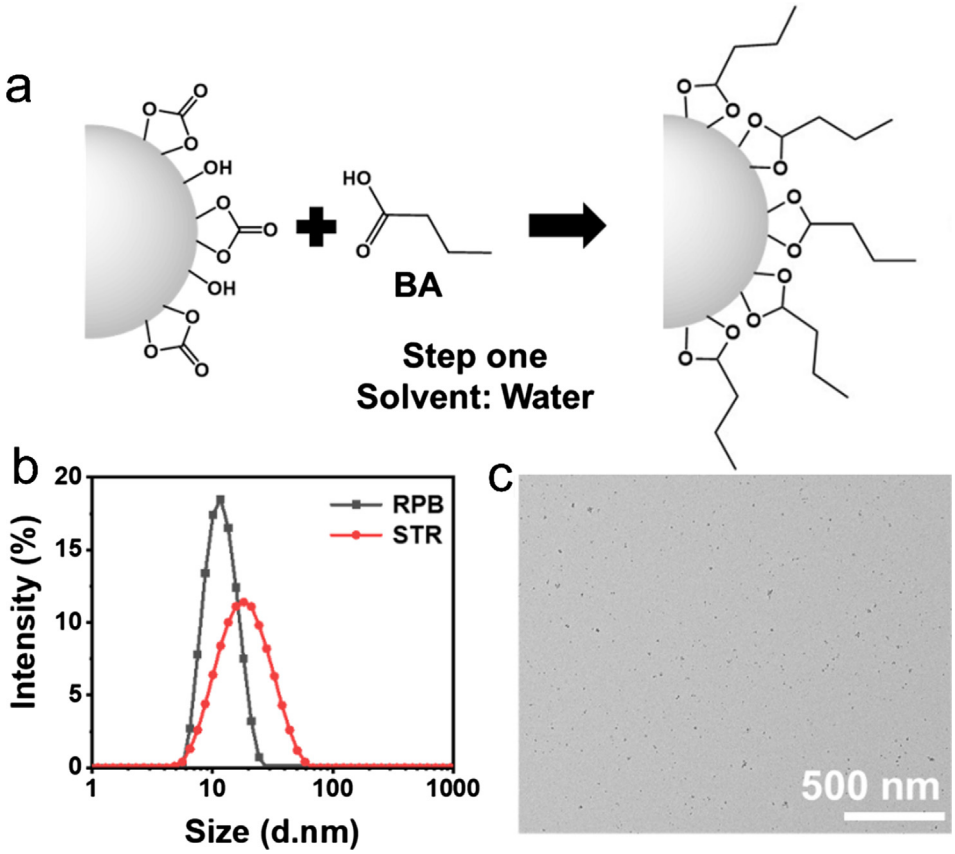

Fig. 4. (a) Schematic diagram of grafting of BA onto ZrO_2 nanoparticles. (b) Hydrodynamic diameters of the ZrO_2@BA nanoparticles obtained from conversional STR route (STR-ZrO_2@BA) and from RPB route (RPB-ZrO_2@BA) in toluene measured by DLS, (c) A typical TEM image of the RPB-ZrO_2@BA nanoparticles.

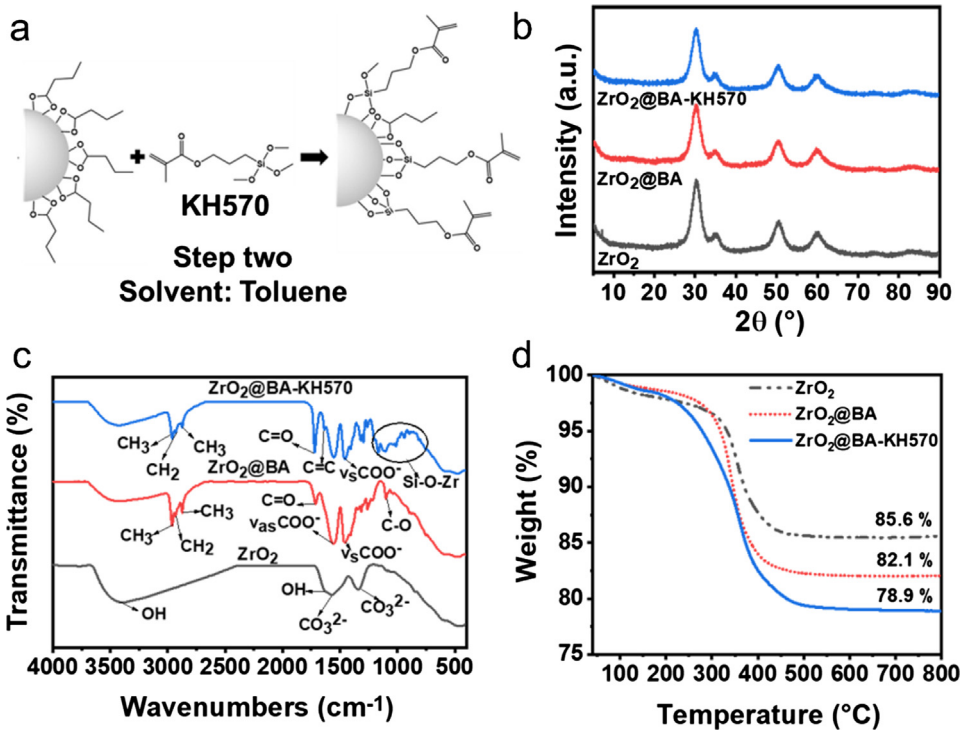

Fig. 5. (a) Schematic diagram of grafting of KH570 onto ZrO_2@BA nanoparticles. (b) XRD, (c) FTIR and (d) TGA characterization ZrO_2, ZrO_2@BA and ZrO_2@BA-KH570 nanoparticles.

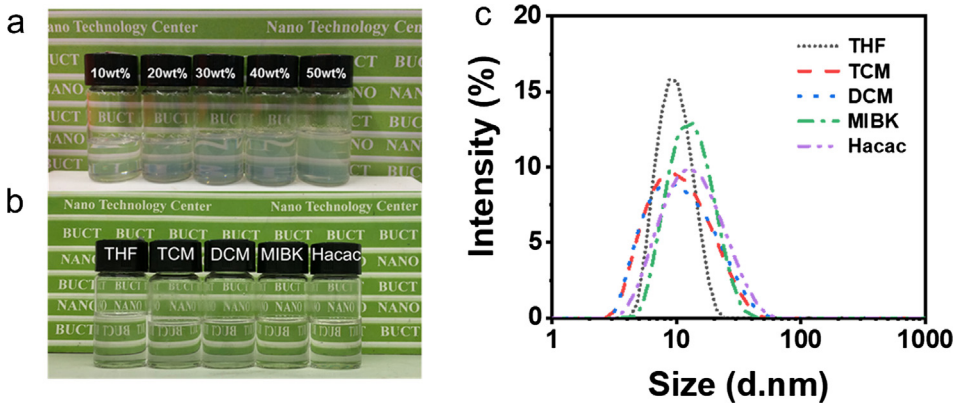

Fig. 6. (a) Photograph of toluene containing ZrO_2@BA-KH570 nanoparticles with solid content of 10, 20, 30, 40, 50 wt%. (b) Photograph of various kinds of organic solvents containing ZrO_2@BA-KH570 nanoparticles with solid content of 5 wt%. (c) Hydrodynamic diameters of the ZrO_2@BA-KH570 nanoparticles in (b) measured by DLS.

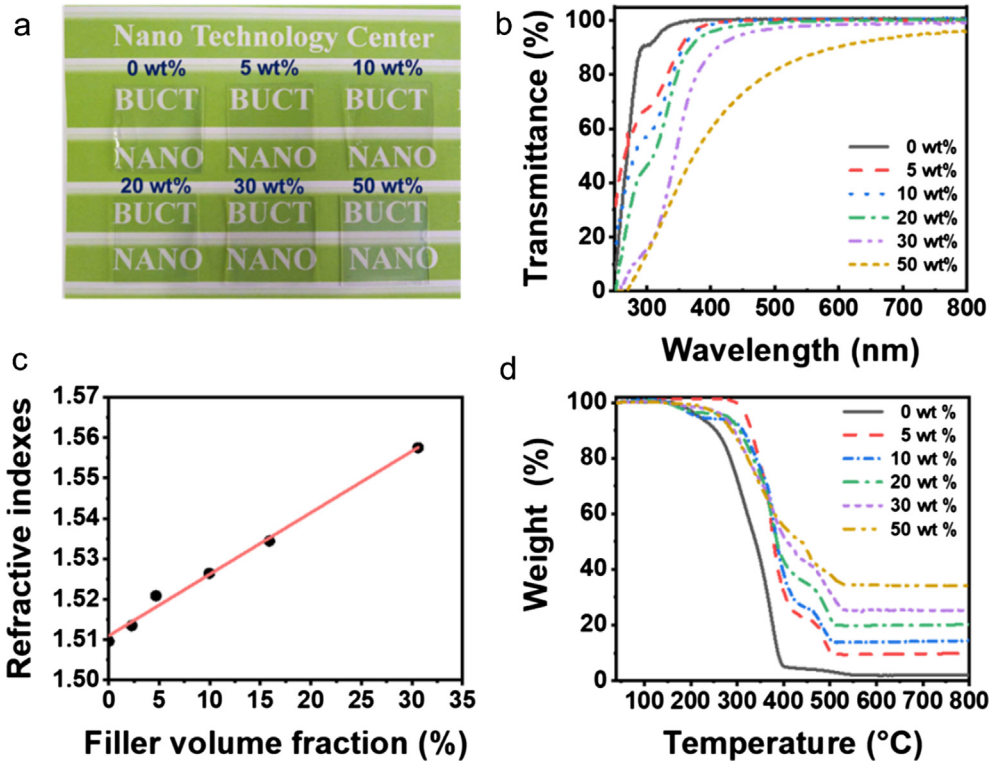

Fig. 7. (a) Digital photos and (b) UV–visible transmittance spectra of ZrO_2/epoxy hybrid nanocomposites containing 0, 5, 10, 20, 30, 50 wt% of ZrO_2@BA-KH570. All the hybrid films were prepared with thickness of 0.25 mm. (c) The refractive indexes@589 nm of the hybrid films as a function of the volume ratio of ZrO_2@BA-KH570 nanoparticles. (d) TGA curves of ZrO_2/epoxy hybrid nanocomposites containing 0, 5, 10, 20, 30, 50 wt% of ZrO_2@BA-KH570 nanoparticles measured in air.

large size aggregates of ZrO_2 in the films. It should be noted that the optical transparency of mixed materials can be estimated using the following equation (Althues et al., 2007; Caseri, 2006; Chau et al., 2007):

$$\frac{I}{I_0} = \exp\left\{-\frac{32\Phi_p x\pi^4 r^3 n_m^4}{\lambda^4}\left[\frac{(n_p/n_m - 1)}{(n_p/n_m + 2)}\right]^2\right\}$$

where r, n_p and Φ_p are the radius, refractive index and fraction of spherical particles, respectively. n_m is the refractive index of matrix. λ is light wavelength, and x is the thickness of the composite. I is the intensity of the transmitted and I_0 of the incident light. One of the most obvious effects is particle size, which is the so-called scattering effect. Because of scattering effect, the transparency of mixed resins can rapidly decay with thickness. Therefore, monodisperse fillers are strongly demanded in order to maintain the high transparency of the composite. Meanwhile, the transparency of a composite is highly related to the thickness of composites. Although some previous reports claimed higher transmittance values of hybrid films with higher ZrO_2 doping ratios (>50 wt%), a closer look at the data often reveals that the thickness of the films are usually low than several μm (Lei et al., 2014; Xia et al., 2018). As for the applications of LED encapsulation, the hybrid films should be thicker than hundreds of μm. In our experiments, the tested films were 0.25 mm in thickness, which are more adaptive to practical application environment. According to a simple estimation of the effective medium theory, the refractive index of a matrix can be calculated by its volume fraction as following (Aspnes, 1982; Yovcheva et al., 2012):

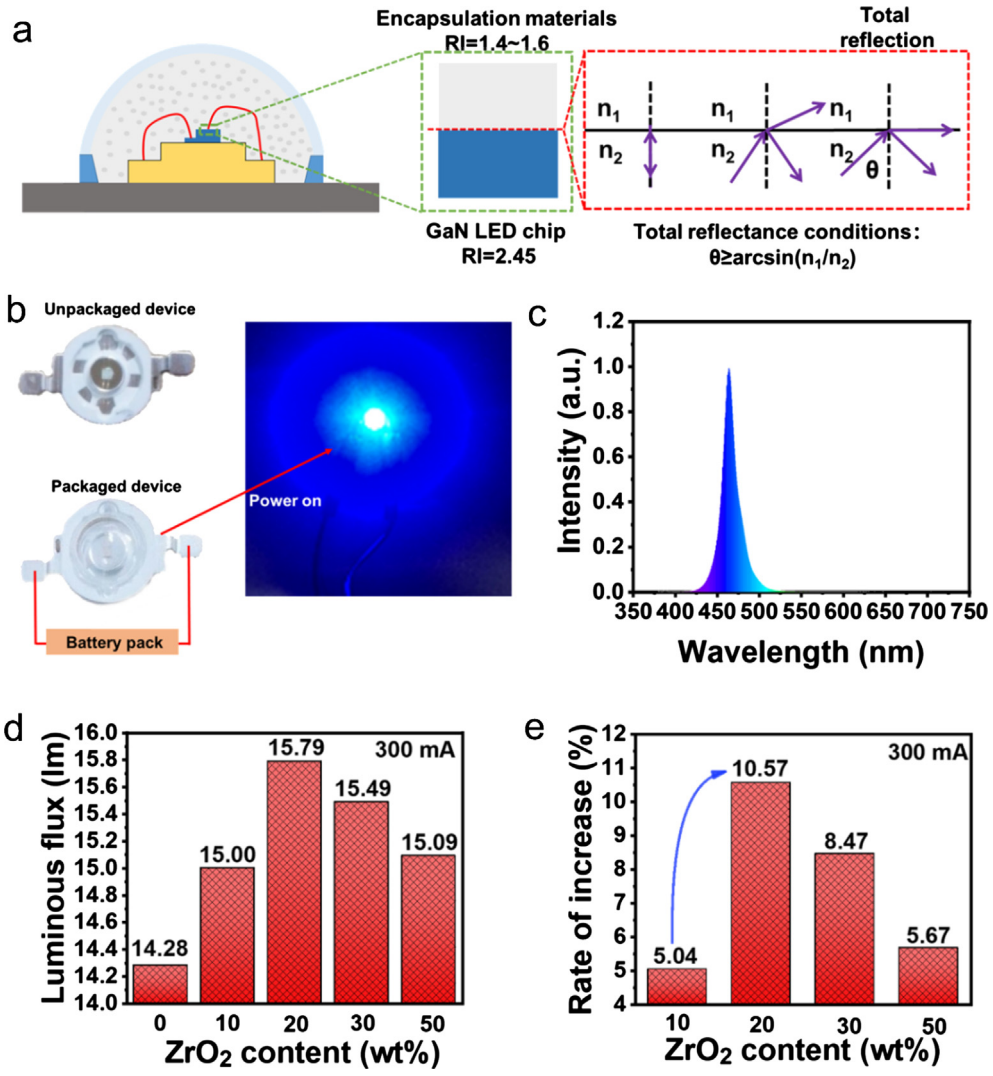

Fig. 8. (a) Schematic diagram of LED encapsulation and the light extraction models at the interface. (b) A typical photo of an illuminated blue LED. (c) Typical spectrum of the blue LED device with ZrO_2/epoxy composite as the encapsulation material. (d) The luminous flux of the LEDs as a function of the ZrO_2 content in the ZrO_2/epoxy encapsulating material at 0, 10, 20, 30 and 50 wt%. (e) The rate of luminous flux increase of LED devices encapsulated with epoxy/ZrO_2 hybrid films with ZrO_2 content of 10, 20, 30 and 50 wt % compare to the devices encapsulated with pure epoxy. (For interpretation of the references to color in this figure legend, the reader is referred to the web version of this article.)

$$\frac{n^2-1}{n^2+2} = \phi_a \frac{n_a^2-1}{n_a^2+2} + \phi_b \frac{n_b^2-1}{n_b^2+2}$$

where n, n_a, n_b are the refractive index of the matrix and that of the components a and b, respectively. The ϕ is the respective volume fractions. The density of the ZrO_2@BA-KH570 is 2.619 g/mL determined by TGA and NMR results. The respective volume fractions of ZrO_2@BA-KH570 were 0, 2.3, 4.7, 9.9, 15.9, 30.6 wt% for the hybrid films with ZrO_2@BA-KH570 weight ratio of 0, 5, 10, 20, 30, 50 wt%. The refractive indexes of various films were measured and the results are presented in Fig. 7c, in which the refractive index of the hybrid film exhibited a significant linear correlation with the content of ZrO_2@BA-KH570 nanoparticles in the range of 0–30.6 wt %. The fitting formulas were obtained as y = 0.00152x + 1.51099 for ZrO_2/epoxy hybrid nanocomposites. The theoretical calculation refractive index of ZrO_2@BA-KH570 nanoparticles is 1.662, which is lower than those of pure bulk ZrO_2 crystals (n = 2.2) (Lu and Yang, 2009). These results were attributed to the effects of surface molecules of BA and KH570 with low refractive index. The thermal stabilities of the various epoxy/ZrO_2 hybrid films were investigated by a TGA analysis. As the results shown in Fig. 7d, the decompose temperature (T*d*) at 10 wt% loss for pure epoxy was around 250 °C, while the T_d values of epoxy/ZrO_2 hybrid films at 10 wt% loss were over 250 °C.

To assess the potential of ZrO_2 nanodispersion for LEDs encapsulation, LEDs devices encapsulated by ZrO_2/epoxy nanocomposites with different ZrO_2 contents were fabricated and the luminous flux values were measured. Fig. 8a shows the schematic diagram of LED encapsulation structure and the schematic diagram of total reflection at its interface. According to Snell's law, a total reflection occurs at the chip encapsulation interface due to the difference of refractive index values between the chip and encapsulation material (Fujii et al., 2004; Huang et al., 2015). In view of this, light produced by LED chip is totally reflected back, or trapped, in other word, inside the chip when the light incident angle is equal or larger than the critical angle, resulting low extraction of light.

$$\theta_c = \arcsin\left(\frac{n_{encapsulation}}{n_{chip}}\right)$$

Therefore, the value of refractive index is one of the most important parameter while evaluating the performance of the encapsulation material to make devices with high light extraction

efficiency. Fig. 8b and c shows the photographs of a typical blue LED device and the spectrum of the light from the chip, respectively. As the results shown in Fig. 8d, the luminous flux of our LEDs devices encapsulated with pure epoxy was 14.28. With the addition of ZrO_2 nanoparticles in the epoxy for encapsulation, the luminous flux of the LEDs was enhanced, which was attributed to the enhanced refractive index values of the encapsulation. A maximum in luminous flux was observed with a value of 15.79 for the LEDs encapsulated with 20 wt% of ZrO_2@BA-KH570 nanoparticles, which was increased by 10.57% compared with the control devices under 300 mA electric current. It was noted that although the hybrid encapsulation films with 30 wt% and 50 wt% of ZrO_2@BA-KH570 exhibited higher refractive index values than the film doped with 20 wt% of ZrO_2@BA-KH570 (Fig. 8d and e), the light extraction efficiency of the devices was lower due to the lower transmittance of the films (Fig. 7b). These experimental results have suggested that ZrO_2 nanodispersion synthesized by the newly developed high-gravity-assisted approach can be used as fillers for potential applications in LEDs encapsulation with enhanced light extraction efficiency.

4. Conclusion

In summary, we develop a novel high-gravity-assisted approach for scalable synthesis of ZrO_2 nanoparticles based on the use of an internal circulation RPB reactor. The optimal conditions for the synthesis of high quality ZrO_2 nanoparticles with average size of 4 nm were confirmed to be work with high gravity level of 182 for 5 h. Followed by a two-step surface modification method for grafting the zirconia nanoparticles with BA and KH570 structures, the ZrO_2 nanoparticles can be dispersed well in organic solvents such as THF, TCM, DCM, MIBK and Hacac with average hydrodynamic size of 10 nm. Furthermore, transparent hybrid encapsulation material of LEDs devices was prepared by doping ZrO_2 nanodispersion in epoxy resin. Compared to the devices encapsulated by pure epoxy, the use of ZrO_2/epoxy hybrid encapsulation benefited the light extraction efficiency of LEDs, increasing up to 10 percent, due to the enhanced refractive index and high transmittance of the hybrid material. This study presents an effective method for highly dispersed sub-10 nm zirconia nanoparticles in moving toward their commercialization and advanced applications in optical devices for saving energy.

Declaration of interests

The authors declared that there is no conflict of interest.

Acknowledgments

We are grateful for financial support from National Key Research and Development Program of China (2017YFB0404302/2017YFB0404300), the National Natural Science Foundation of China (21808009, 21620102007, 21622601) and the Beijing Natural Science Foundation (2182051).

Appendix A. Supplementary material

Supplementary data to this article can be found online at https://doi.org/10.1016/j.ces.2018.11.036.

References

Althues, H., Henle, J., Kaskel, S., 2007. Functional inorganic nanofillers for transparent polymers. Chem. Soc. Rev. 36, 1454–1465.
Aspnes, D.E., 1982. Local-field effects and effective-medium theory: a microscopic perspective. Am. J. Phys. 50, 704–709.
Caseri, W.R., 2006. Nanocomposites of polymers and inorganic particles: preparation, structure and properties. Mater. Sci. Technol.-Lond. 22, 807–817.
Chang, Y., Dong, S., Wang, H., Du, K., Zhu, Q., Luo, P., 2012. Synthesis of monodisperse spherical nanometer ZrO_2 (Y_2O_3) powders via the coupling route of w/o emulsion with urea homogenous precipitation. Mater. Res. Bull. 47, 527–531.
Chau, J.L.H., Lin, Y.M., Li, A.K., Su, W.F., Chang, K.S., Hsu, S.L.C., Li, T.L., 2007. Transparent high refractive index nanocomposite thin films. Mater. Lett. 61, 2908–2910.
Chen, J.F., 2017. Green chemical engineering for a better life. Engineering 3. 279-279.
Chen, L., Zhang, C., Du, Z., Li, H., Zhang, L., Zou, W., 2015. Synthesis of poly(n-butyl methacrylate)-(glycidyl methacrylate) block copolymer and its compatibilization at the interface of the QD/epoxy nanocomposite for white LED encapsulation. RSC Adv. 5, 65184–65191.
Chiang, A.S.T., Wang, S.H., Pai, C.T., Chen, C.W., 2016. Metal oxide nanoparticle material, U.S. Patent Application 20160096738 A1, April 7.
Chiang, A.S.T., 2015. The production of dispersible zirconia nanocrystals: a recent patent review. Recent Innov. Chem. Eng. (Formerly Recent Patents on Chemical Engineering) 7, 76–95.
Chung, P.T., Chiou, S.H., Tseng, C.Y., Chiang, A.S.T., 2016. Preparation and evaluation of a zirconia/oligosiloxane nanocomposite for LED encapsulation. ACS Appl. Mater. Inter. 8, 9986–9993.
Chung, P.T., Yang, C.T., Wang, S.H., Chen, C.W., Chiang, A.S.T., Liu, C.Y., 2012. ZrO_2/epoxy nanocomposite for LED encapsulation. Mater. Chem. Phys. 136, 868–876.
Enomoto, K., Ichijo, Y., Nakano, M., Kikuchi, M., Narumi, A., Horiuchi, S., Kawaguchi, S., 2017. Unique hydrophobization and hybridization via direct phase transfer of ZrO_2 nanoparticles from water to toluene producing highly transparent polystyrene and poly(methyl methacrylate) hybrid bulk materials. Macromolecules 50, 9713–9725.
Enomoto, K., Kikuchi, M., Narumi, A., Kawaguchi, S., 2015. Design of epoxy/ZrO_2 hybrid transparent bulk materials. Kobunshi Ronbunshu 72, 82–89.
Enomoto, K., Kikuchi, M., Narumi, A., Kawaguchi, S., 2018. Surface modifier-free organic-inorganic hybridization to produce optically transparent and highly refractive bulk materials composed of epoxy resins and ZrO_2 nanoparticles. ACS Appl. Mater. Inter. 10, 13985–13998.
Fujii, T., Gao, Y., Sharma, R., Hu, E.L., DenBaars, S.P., Nakamura, S., 2004. Increase in the extraction efficiency of GaN-based light-emitting diodes via surface roughening. Appl. Phys. Lett. 84, 855–857.
Garnweitner, G., Goldenberg, L.M., Sakhno, O.V., Antonietti, M., Niederberger, M., Stumpe, J., 2007. Large-scale synthesis of organophilic zirconia nanoparticles and their application in organic-inorganic nanocomposites for efficient volume holography. Small 3, 1626–1632.
Huang, F., Chen, D., Zhou, J., Wang, Y., 2011. Modifying the phase and controlling the size of monodisperse ZrO_2 nanocrystals by employing Gd^{3+} as a nucleation agent. CrystEngCommun. 13, 4500–4502.
Huang, J.H., Li, C.P., Chang-Jian, C.W., Lee, K.C., Huang, J.H., 2015. Preparation and characterization of high refractive index silicone/TiO_2 nanocomposites for LED encapsulants. J. Taiwan Inst. Chem. E. 46, 168–175.
Huang, P., Shi, H.Q., Xiao, H.M., Li, Y.Q., Hu, N., Fu, S.Y., 2017. High performance surface-modified TiO_2/silicone nanocomposite. Sci. Rep. 7, 5951.
Huang, X.J., Zeng, X.F., Wang, J.X., Chen, J.F., 2018. Transparent dispersions of monodispersed ZnO nanoparticles with ultrahigh content and stability for polymer nanocomposite film with excellent optical properties. Ind. Eng. Chem. Res. 57, 4253–4260.
Jiao, W., Qin, Y., Luo, S., He, Z., Feng, Z., Liu, Y., 2017. Simultaneous formation of nanoscale zero-valent iron and degradation of nitrobenzene in wastewater in an impinging stream-rotating packed bed reactor. Chem. Eng. J. 321, 564–571.
Kang, F., Wang, D., Pu, Y., Zeng, X.F., Wang, J.X., Chen, J.F., 2018. Efficient preparation of monodisperse $CaCO_3$ nanoparticles as overbased nanodetergents in a high-gravity rotating packed bed reactor. Powder Technol. 325, 405–411.
Kuang, Y.Y., Zhang, Z.B., Xie, M.L., Wang, J.X., Le, Y., Chen, J.F., 2015. Large-scale preparation of amorphous cefixime nanoparticles by antisolvent precipitation in a high-gravity rotating packed bed. Ind. Eng. Chem. Res. 54, 8157–8165.
Lee, S., Shin, H.J., Yoon, S.M., Yi, D.K., Choi, J.Y., Paik, U., 2008. Refractive index engineering of transparent ZrO_2-polydimethylsiloxane nanocomposites. J. Mater. Chem. 18, 1751–1755.
Lei, I.A., Lai, D.F., Don, T.M., Chen, W.C., Yu, Y.Y., Chiu, W.Y., 2014. Silicone hybrid materials useful for the encapsulation of light-emitting diodes. Mater. Chem. Phys. 144, 41–48.
Leng, J., Chen, J., Wang, D., Wang, J.X., Pu, Y., Chen, J.F., 2017. Scalable preparation of Gd_2O_3:Yb^{3+}/Er^{3+} upconversion nanophosphors in a high-gravity rotating packed bed reactor for transparent upconversion luminescent films. Ind. Eng. Chem. Res. 56, 7977–7983.
Li, W., Huang, H., Li, H., Zhang, W., Liu, H., 2008. Facile synthesis of pure monoclinic and tetragonal zirconia nanoparticles and their phase effects on the behavior of supported molybdena catalysts for methanol-selective oxidation. Langmuir 24, 8358–8366.
Lin, Y.T., Li, Y.H., Lei, I.A., Kuo, C.Y., Lee, C.F., Chiu, W.Y., Don, T.M., 2018. Enhanced reliability of LEDs encapsulated with surface-modified zirconia/silicone hybrids under thermal shock. Mater. Chem. Phys. 206, 136–143.
Lu, C., Yang, B., 2009. High refractive index organic-inorganic nanocomposites: design, synthesis and application. J. Mater. Chem. 19, 2884–2901.
Pu, Y., Cai, F., Wang, D., Wang, J.X., Chen, J.F., 2018a. Colloidal synthesis of semiconductor quantum dots toward large scale production: a review. Ind. Eng. Chem. Res. 57, 1790–1802.

Pu, Y., Leng, J., Wang, D., Wang, J.X., Foster, N.R., Chen, J.F., 2018b. Process intensification for scalable synthesis of ytterbium and erbium co-doped sodium yttrium fluoride upconversion nanodispersions. Powder Technol. 340, 208–216.
Singhal, A., Toth, L.M., Lin, J.S., Affholter, K., 1996. Zirconium(IV) tetramer/octamer hydrolysis equilibrium in aqueous hydrochloric acid solution. J. Am. Chem. Soc. 118, 11529–11534.
Su, H.W., Chen, W.C., 2008. Photosensitive high-refractive-index poly(acrylic acid)-graft-poly(ethylene glycol methacrylate) nanocrystalline titania hybrid films. Macromol. Chem. Phys. 209, 1778–1786.
Tao, P., Li, Y., Siegel, R.W., Schadler, L.S., 2013. Transparent dispensible high-refractive index ZrO_2/epoxy nanocomposites for LED encapsulation. J. Appl. Polym. Sci. 130, 3785–3793.
Wang, D., Wang, Z., Zhan, Q., Pu, Y., Wang, J.X., Foster, N.R., Dai, L., 2017. Facile and scalable preparation of fluorescent carbon dots for multifunctional applications. Engineering 3, 402–408.
Wenzel, D., Gorak, A., 2018. Review and analysis of micromixing in rotating packed beds. Chem. Eng. J. 345, 492–506.
Wu, K., Wu, H., Dai, T., Liu, X., Chen, J.F., Le, Y., 2018. Controlling nucleation and fabricating nanoparticulate formulation of sorafenib using a high-gravity rotating packed bed. Ind. Eng. Chem. Res. 57, 1903–1911.
Wu, K., Xie, M.L., Chen, J.F., Le, Y., 2016. A novel routine for the fabrication of Y-type oxotitanium phthalocyanine nanocrystals in high-gravity rotating packed beds. Ind. Eng. Chem. Res. 55, 6753–6759.
Xia, Y., Zhang, C., Wang, J.X., Wang, D., Zeng, X.F., Chen, J.F., 2018. Synthesis of transparent aqueous ZrO_2 nanodispersion with a controllable crystalline phase without modification for a high-refractive-index nanocomposite film. Langmuir 34, 6806–6813.
Yamada, N., Yoshinaga, I., Katayama, S., 2000. Formation behavior and optical properties of transparent inorganic-organic hybrids prepared from metal alkoxides and polydimethylsiloxane. J. Sol-Gel Sci. Technol. 17, 123–130.
Yang, X., Leng, J., Wang, D., Wang, Z., Wang, J.X., Pu, Y., Shui, J., Chen, J.F., 2017. Synthesis of flower-shaped V_2O_5:Fe^{3+} microarchitectures in a high-gravity rotating packed bed with enhanced electrochemical performance for lithium ion batteries. Chem. Eng. Process. 120, 201–206.
Yovcheva, T., Vlaeva, I., Bodurov, I., Dragostinova, V., Sainov, S., 2012. Refractive index investigation of poly(vinyl alcohol) films with TiO_2 nanoparticle inclusions. Appl. Optics. 51, 7771–7775.
Zhao, H., Shao, L., Chen, J.F., 2010. High-gravity process intensification technology and application. Chem. Eng. J. 156, 588–593.
Zhao, Z., Wang, Z., Wang, D., Wang, J.X., Foster, N.R., Pu, Y., Chen, J.F., 2018. Preparation of 3D graphene/iron oxides aerogels based on high-gravity intensified reactive precipitation and their applications for photo-Fenton reaction. Chem. Eng. Process. 129, 77–83.